Stem cell-derived cardiomyocyte migration through TGF-β signalling in the context of myocardial infarction

Laura Deelen, Kazuya Kobayashi, Alia Hafiz Abbas Gasim, Fiona Lewis-McDougall*, Ken Suzuki*

Centre for Microvascular Research, William Harvey Research Institute, Faculty of Medicine and Dentistry, Queen Mary University of London, UK

*Joint corresponding authors: f.lewis@qmul.ac.uk, ken.suzuki@qmul.ac.uk

This study was funded by the British Heart Foundation (MRes/PhD DTP Programme, FS/19/62/34901).

ABSTRACT

Cardiac regeneration using human induced pluripotent stem cell-derived cardiomyocytes (hiPSC-CMs) is a promising therapy for heart failure. Successful treatment requires effective integration of transplanted cells with host myocardium, yet the migratory capacity of hiPSC-CMs remains poorly understood. This study investigated hiPSC-CM migration using *in vitro* models with myocardial infarction (MI) stimulus mimicked using homogenised rat MI tissue. Transwell assays revealed a concentration-dependent chemotactic response, with a three-fold increase in migration toward MI homogenate. Wound healing assays confirmed enhanced migration speed under MI conditions. Bulk RNA sequencing identified TGF-β signalling as a key regulatory pathway, and both pharmacological inhibition and antibody neutralisation of TGF-β significantly impaired migration. These findings demonstrate the inherent chemotactic ability of hiPSC-CMs and identify TGF-β signalling as a central mediator in response to MI stimuli. This work provides new mechanistic information on hiPSC-CM migratory behaviour in the context of MI and offers new insights to optimise cardiac regeneration therapies.

INTRODUCTION

Myocardial infarction (MI) is one of the most common causes of ischaemic heart failure (HF), for which the prognosis is only 50% within 5 years of diagnosis[1]. During MI, persistent coronary artery obstruction leads to the irreversible loss of billions of cardiac cells including cardiomyocytes (CMs). Currently the only established treatment for end-stage HF patients is heart transplantation or the permanent implantation of a left ventricular assist device as an emerging alternative[2,3]. However, these approaches have several limitations, including high costs, complications related to immunosuppression or anticoagulants, and psychological strain for patients. Myocardial regeneration therapy has drawn major attention over the last few decades as an innovative treatment to restore functional CMs after MI and improve prognosis through enhanced cardiac function. Human induced pluripotent stem cells (hiPSCs) have gained popularity as donor cells for myocardial regeneration therapy due to their unlimited self-renewal, autologous clinical potential and robust cardiomyogenic differentiation potency. Therefore, the transplantation of hiPSC-derived CMs (hiPSC-CMs) has become an active field of research for the treatment of post-MI HF.

Promising methods for delivery of replacement CMs to the heart include epicardial placement as a patch and intramyocardial injection of cell suspension or spheroids[4–6]. Migration of hiPSC-CMs post-transplantation is key to future success of these therapies. It is reported that many donor cells remain on the heart surface post-epicardial placement[7,8]. However, if transplanted CMs could migrate into the myocardium and establish cell-cell connections with donor CMs, this would undoubtedly enhance cardiac contractility. Intramyocardial injection can directly deliver hiPSC-CMs to the targeted area however migration to host surviving CMs is still required. So far, little is known about the intrinsic migration ability of hiPSC-CMs, with limited studies exploring this phenomenon. Moyes et al. assessed the migratory potential of hESC-CMs *in vitro* and found a migratory effect of Wnt5a and fibronectin[9]. Another study showed

that BANCR, a long non-coding RNA specific to primates, has a migratory effect for hiPSC-CMs[10]. Further studies on CM migration have focused on embryonic or neonatal CM migration and have indicated non-coding RNAs as well as proteins activated in cardiogenesis can affect CM migration[11–14]. One of the pathways that has been linked to CM migration during regeneration of the damaged heart is the TGF-β signalling pathway. In the regenerative zebrafish model, heart regeneration is dependent on SMAD3-dependent TGF-β signalling, and inhibition of TGF-β signalling using the chemical inhibitor SB431542 impaired the migration of CMs into the damaged tissue[15]. Researchers have further shown that inhibiting TGF-β-Smad3 signalling inhibits an EMT-like response in CMs during myocardial regeneration after ablation in zebrafish[16]. We know that an array of molecules are released from the injured myocardium, and we hypothesise that a key molecules may serve as migratory signals to stimulate the movement of CMs and resultant cardiac regeneration similar to what is observed in the zebrafish model[17]. In the injured heart, adult CMs are likely to have lost the ability to respond to these signals, however, due to the close resemblance of hiPSC-CMs to embryonic or fetal CMs, they may possess a similar intrinsic migration ability.

In this paper, we aim to explore the migratory abilities of hiPSC-CMs and their response to signals present in the infarcted microenvironment. For this purpose, we utilised transwell migration and wound healing assays to investigate hiPSC-CM response to rat MI tissue homogenate and migration speed. Furthermore, we aimed to explore the underlying signalling mechanisms through RNA sequencing of migrated hiPSC-CMs and non-migrated counterparts. Together, the unique combination of our hiPSC-CM transwell migration model and *in vitro* exposure to rat MI myocardium homogenate provides novel information on the inherent migration capacity of hiPSC-CMs and their behaviour in the context of MI, which can be used to modulate their migratory response and further enhance current potential cell therapies for post-MI treatment.

RESULTS

HiPSC-CMs exhibit a concentration-dependent chemotactic response to rat MI tissue homogenate

Four hiPSC lines (hiPSC-A, B, C and D) were used in this study, all which were confirmed to express surface and intracellular pluripotency markers and were karyotypically normal (Fig. S1). To generate hiPSC-CMs, we utilised the well-established protocol published by Burridge et. al[18] or a commercially produced CM Differentiation Kit (STEMCELL Technologies) as an alternative. The first spontaneous cell contractions were observed between 7 and 11 days after the start of differentiation (Vid. S1). Additionally, flow cytometry, RT-PCR, and immunofluorescence staining were used to analyse the efficiency of cardiomyogenic differentiation of hiPSCs. The Burridge protocol led to consistent cTnT expression in all four hiPSC lines (Fig. S2A) with cTnT, Nkx2.5 and alpha-actinin protein expression confirmed at day 15 of differentiation (Fig. S2B). HiPSCs differentiated with either protocol showed downregulation in gene expression of pluripotency markers *POU5F1*, *NANOG*, *SOX2*, transient upregulation of *MESP1* and *KIT* and upregulation of CM markers *NKX2-5, TNNT2, MYL7, MYL2* during the differentiation time course (Fig. S2C-G). To evaluate the efficiency of cardiomyocyte differentiation, we performed flow cytometry to determine the percentage of cells expressing cardiac troponin T (cTnT), a marker of cardiac lineage commitment. We used a threshold of 60% cTnT in all cases before proceeding to use hiPSC-CMs in downstream experiments.

To assess whether an MI stimulus has a chemotactic effect on hiPSC-CMs, a transwell migration (TWM) assay was designed (Fig. 1A). HiPSC-CM-A were seeded in the upper chamber of the transwell and exposed to different dilutions of MI myocardium homogenate, obtained from the rat left ventricular (LV) myocardium 1-day post-MI. After 24 hours a

99 considerable number of hiPSC-CMs migrated through the membrane (Fig. 1B-D). Migrated
100 hiPSC-CMs were detected by DAPI staining on the lower surface of the membrane and
101 quantified. We observed a significant increase in the number of migrated hiPSC-CMs when
102 exposed to MI homogenate, compared to cell medium, in a dose-responsive manner (1:10 –
103 1:50 dilution; Fig. 1C). The increase in migration reached 3-fold at a dilution of 1:10. Similarly,
104 hiPSC-CM-B exhibited a significant 3-fold increase in migration when incubated with MI
105 homogenate at a 1:10 dilution compared to cell medium, and an increasing trend was observed
106 at MI dilutions of 1:20 ($p = 0.05$) and 1:5 ($p = 0.07$) (Fig. 1D). Similar results were obtained
107 for hiPSC-CM-C (Fig. S3). An additional objective of this study was to examine whether
108 extended culture of hiPSC-CMs leads to a change in their migration capability, an important
109 consideration as it is known that prolonged culture promotes maturation of these cells, which
110 likely impacts their migratory capacity[19,20]. We hypothesised that hiPSC-CM migration ability
111 would diminish over time in culture, given that mature CMs typically exhibit non-migratory
112 behaviour. When hiPSC-CMs, maintained for varying culture periods, were exposed to MI
113 homogenate, cell line-specific variations in their migratory capacity were seen up to day 45 of
114 differentiation culture (Fig. 1E-F). We observed an average of 28-30% migration for hiPSC-
115 CM-A and hiPSC-CM-B at day 15 of differentiation. Interestingly, for hiPSC-CM-A, no
116 significant changes in migratory ability were detected through prolonged culture (Fig. 1E).
117 Despite a suggested decrease in migration at day 30, hiPSC-CM-A maintained a migratory
118 ability of 20-30% from day 15 up to day 45 of differentiation. In contrast, for hiPSC-CM-B, a
119 significant decline in the percentage of migratory cells was seen over time, reducing to 9% at
120 day 45, in accordance with the expected trend (Fig. 1F). These results highlight cell line-
121 specific differences, which require further investigation. Taken together, the results of our
122 TWM assays reveal a concentration-dependent chemotactic effect of MI homogenate that
123 stimulates hiPSC-CM migration in multiple hiPSC lines. However, migratory capacity appears

124 to be influenced by cell line-specific and temporal factors, underscoring the importance of
125 considering these variables in regenerative applications.

126 ***MI Stimulus Accelerates Collective hiPSC-CM Migration***

127 To further elucidate the effect of an MI stimulus on hiPSC-CM migration in a different model,
128 we assessed the wound closure and cell front migration speed of hiPSC-CM-D after incubation
129 with LV myocardium homogenate from rats with or without MI (Fig. 2A-C). After 4 hours of
130 incubation following scratch generation on the monolayer of hiPSC-CMs, we observed a
131 significant increase in wound closure of hiPSC-CMs when exposed to MI homogenate (1:10
132 dilution; 16.6 ± 6.9 %) compared to cell medium (8.5 ± 5.2 %). In terms of cell front migration
133 speed, hiPSC-CMs incubated with cell medium alone travelled an average of 6.2 ± 3.7 μm/h
134 over the course of 4 hours, comparable to a previously reported migration study on hESC-
135 CMs[9]. The cell front migration speed more than doubled to 14.3 ± 4.4 μm/h when incubated
136 with MI homogenate (1:10 dilution).

137 Interestingly, increased wound closure (14.7 ± 4.6 %) and cell front migration speed (11.2 ±
138 4.0 μm/h) of hiPSC-CMs were also observed when incubated with non-MI sham LV
139 homogenate (Fig. 2A-C) albeit to a lower extent. This was further explored in a TWM assay,
140 in which a non-MI homogenate caused a significant increase in hiPSC-CM migration, yet a
141 lower fold change than MI homogenate (Fig. 2D). The homogenisation process itself likely
142 influenced the chemokinetic effect of the non-MI sham LV homogenate by artificially releasing
143 intracellular contents, which can stimulate cell migration. While MI naturally causes such
144 release through necrosis, it should be minimal in intact myocardium. Thus, the non-MI sham
145 group may not fully represent normal myocardium. Nevertheless, these results suggest that
146 there are unique chemokinetic factors present within a rat MI homogenate that robustly

147 stimulate hiPSC-CMs migration above that of the background factors generated as part of the
148 homogenisation process.

149 ***Migrated hiPSC-CMs exhibit a differential gene expression profile from non-migrated***
150 ***hiPSC-CMs***

151 To investigate which pathways are involved in hiPSC-CM migration, we used a TWM assay
152 in which day 15 hiPSC-CMs were exposed to MI homogenate for 24 hours. We then collected
153 migrated hiPSC-CMs from the lower surface of the membrane and non-migrated hiPSC-CMs
154 from the upper surface. RNA was extracted from these cells in parallel for bulk RNAseq to
155 investigate gene expression differences in a comprehensive manner. Principal component
156 analysis revealed distinct segregation between the hiPSC-CM-A and hiPSC-CM-B lines and
157 between migrated and non-migrated samples of each line along PC1 and PC2, respectively
158 (Fig. 3A). These top two principal components captured 91.53% of the data, indicating that
159 these features account for the vast majority of the variation within the dataset. Overall, those
160 gene expression changes were greater for hiPSC-CM-A than hiPSC-CM-B. This distribution
161 suggests that a large proportion of the variation in the data may be explained by the differences
162 in donor cell background, emphasising general inter-line variability.

163 To validate our assay, we investigated the expression of CM markers of the migrated and non-
164 migrated hiPSC-CMs from each cell line. Both cell lines expressed CM markers (*TNNT2*,
165 *NKX2-5*, *MYL7*) at similar levels in the migrated and non-migrated groups (Table S1). In terms
166 of CM subtypes, we observed a mixture of atrial (*NR2F2*), ventricular (*MYL2*, *IRX4*) and nodal
167 (*TBX18*, *HCN4*) subtypes at both timepoints (Table S1), consistent with the expected outcome
168 of the Burridge *et al.* protocol (Fig. S2). The immature nature of the hiPSC-CMs was reflected
169 in the higher expression of *TNNI1* compared to *TNNI3* and higher expression of *MYH6*
170 compared to *MYH7* (Table S1). We next investigated the presence of any non-CM populations

171 in our samples but only observed relatively low expression of the cardiac fibroblast markers
172 DDR2 and CD90 (*THY1*) compared to CM markers, and no detectable expression of the
173 endothelial marker CD31 was observed in either cell line (Table S1). Furthermore, we observed
174 substantial expression of alpha smooth muscle actin (*ACTA2*), which is typically a marker of
175 vascular smooth muscle cells and myofibroblasts, however, this gene has also been shown to
176 be expressed in hiPSC-CMs and emphasises the immaturity of CMs[21,22].

177 After 24 hours of incubation with MI homogenate, RNAseq analysis revealed that 849 genes
178 were differentially expressed in migrated hiPSC-CM-A compared to non-migrated hiPSC-CM-
179 A, of which 598 were significantly upregulated and 248 were downregulated (padj < 0.05,
180 log2FC > |1|) (Fig. 3B). Similarly, 46 genes showed significant differential expression in
181 migrated versus non-migrated hiPSC-CM-B, of which 38 were upregulated and 8 were
182 downregulated. The difference in number of differentially expressed genes (DEGs) between
183 these two cell lines correlates to the greater distance between the non-migrated and migrated
184 cells of hiPSC-CM-A than those of hiPSC-CM-B shown in the PCA plot. Combining the
185 datasets of the two hiPSC-CM lines rendered a panel of 28 DEGs (Fig. 3C-D). We chose 14
186 genes of interest from this combined panel and further verified their upregulation in three
187 different hiPSC lines by RT-qPCR highlighting the reproducibility of our findings (Fig. S4).
188 Gene Ontology (GO) analysis revealed that genes enriched in our study are linked to the
189 biological processes of extracellular matrix organisation, cell migration or chemotaxis (Table
190 S2). We further analysed the RNAseq data using Ingenuity Pathway Analysis (IPA, QIAGEN),
191 which indicated that cellular movement as one of the top cellular and molecular functions
192 associated with both datasets (Fig. 3F) providing evidence that our unique model is capable of
193 deciphering regulators of hiPSC-CM migration.

194

195 ***Inhibition of TGF-β signalling decreases MI homogenate-induced hiPSC-CM migration***

196 To identify one or multiple upstream regulators that may have induced hiPSC-CM migration,
197 we explored links between the DEGs of the RNAseq datasets. Seven out of 28 DEGs shared
198 between migrated hiPSC-CM-A and hiPSC-CM-B (*SOX17, BMP6, TGFBI, SPP1, NT5E,*
199 *HMGA2* and *DACT2*) were directly associated with TGF-β signalling[23–28]. In addition,
200 Ingenuity Pathway Analysis (Qiagen) identified an associative link between 12 DEGs and
201 TGF-β1. TGF-β signalling is known to be upregulated in the myocardium after MI[29,30].
202 Furthermore, it plays a key role in the regenerative capacity of the heart in zebrafish[15],
203 including the epithelial-to-mesenchymal (EMT)-like response of CMs, wherein they display a
204 migratory profile[16]. TGF-β has previously been shown to elicit an EMT response through
205 HMGA2, one of the DEGs from our panel[28].

206 Based on this information, we further investigated the role of TGF-β signalling in hiPSC-CM
207 migration by using the pharmacological inhibitor SB431542, which inhibits the kinase activity
208 of the TGF-β type I receptor (ALK5)[31]. Utilising a scratch wound assay, we identified that the
209 addition of SB431542 to MI homogenate from 1h up to 20h after incubation decreased wound
210 closure, suggesting that TGF-β signalling is involved in MI-homogenate induced hiPSC-CM
211 migration (Fig. 4A). In addition, the cell front migration velocity was also decreased over the
212 course of 24 hours to the basal level of hiPSC-CMs incubated with medium alone (Fig. 4B).
213 Notably, cell front migration velocity was significantly reduced in the presence of SB431542
214 compared to MI homogenate alone from 1 to 8 hours of incubation, indicating an early role of
215 TGF-β signalling in regulating hiPSC-CM migration. Together these data indicate that
216 SB431542 attenuated the migration induced by MI homogenate and suggest that the duration
217 of the migratory stimulus within the MI homogenate is short-lived, acting within the first few
218 hours of incubation.

219 We further investigated the role of TGF-β signalling in hiPSC-CM migration. We confirmed
220 the presence of TGF-β1 protein in MI homogenate (1,014 ± 183 ng/mL), which was
221 significantly greater than the non-MI sham homogenate (540 ± 146 ng/mL, Fig. S5). The
222 presence of TGF-β1 albeit at lower levels may explain the chemokinetic and chemotactic effect
223 of sham homogenate on hiPSC-CM migration observed (Fig. 2). Next, we used a TWM assay
224 to investigate the effect of TGF-β signalling inhibition. After 4 hours of incubation, we
225 observed a significant decrease in the number of migrated hiPSC-CMs upon introduction of
226 10μM SB431542 to the MI homogenate (Fig. 4C-D). Similarly, we investigated the role of
227 TGF-β in hiPSC-CM migration by applying a neutralising TGF-β antibody. For hiPSC-CM-A,
228 this treatment significantly reduced MI homogenate-induced migration (Fig. 4E). While
229 hiPSC-CM-B also exhibited a strong decreasing trend in migration after 4 hours of incubation
230 with the neutralising antibody alongside MI homogenate ($p = 0.05$). Taken together, these
231 findings suggest that TGF-β1 in MI homogenate plays a key role in promoting hiPSC-CM
232 migration, as its inhibition or neutralisation significantly reduces the migratory response.

233 **DISCUSSION**

234 This study primarily aimed to characterise the migratory ability of hiPSC-CMs when exposed
235 to factors from an infarcted myocardium, representing, to the best of our knowledge, the first
236 investigation of its kind. Two gold-standard techniques verified the migratory effect of an MI
237 stimulus on hiPSC-CM migration, utilising different hiPSC lines to ensure biological
238 reproducibility. A TWM model unveiled significant concentration-dependent chemotactic
239 responses of hiPSC-CMs to rat MI myocardium homogenate, while a scratch wound assay
240 consistently demonstrated a significant increase in wound closure as well as migration speed
241 of hiPSC-CMs upon exposure to MI homogenate. These results reveal a previously unknown
242 biological characteristic of hiPSC-CMs in the context of MI.

243 Our TWM model enabled us to isolate migrated hiPSC-CMs and non-migrated hiPSC-CMs
244 due to the physical separation of these populations. RNAseq of migrated and non-migrated
245 hiPSC-CMs revealed differential gene expression potentially implicated in migration. The role
246 of one of these, TGF-β was confirmed through inhibition studies, which demonstrated a
247 reduction in MI homogenate-induced migration of hiPSC-CMs. TGF-β has been proposed as a
248 chemoattractant for over two decades[32,33] and has been shown to play a role in migration for a
249 range of different cell types[34–36]. Its significance in cell migration within the cardiac context
250 has previously been shown during heart development as well as in the adult heart[37]. In the
251 context of heart regeneration, the role of TGF-β has been well established in zebrafish. Upon
252 cryoinjury, TGF-β is released and binds the TGFBR1 receptor on fibroblasts and cardiac cells[15].
253 A temporary scar is initially formed, which was later replaced by new CMs originating from
254 the proliferation and migration of existing CMs, in which the authors demonstrated the
255 involvement of TGF-β in this process. Further research in zebrafish has shown that TGF-β
256 exhibits an EMT-like response in CMs[16]. In mammals, it is well-documented that TGF-β is
257 upregulated after MI [29,30], which correlates with our findings. The TGF-β response after MI has

258 been shown to involve numerous processes, such as CM survival, hypertrophy, immune cell
259 regulation and fibroblast activation[38]. Importantly, the mode of action of the TGF-β family has
260 been demonstrated to be context-dependent, as both proliferative and anti-proliferative effects
261 on cardiac fibroblasts have been reported[39,40], as well as both angiogenic and angiostatic
262 outcomes[41]. Our results encourage further exploration of TGF-β signalling to enhance or
263 regulate intra-cardiac migration of hiPSC-CMs after transplantation for the treatment of MI,
264 which will result in enhancement of therapeutic efficacy of this type of approach. However, in
265 such treatment, it will be important to be cautious about the context-dependent effects of TGF-
266 β, potentially exerting both protective and damaging effects.

267 Interestingly, key genes involved in cell proliferation were significantly upregulated in
268 migrated hiPSC-CMs in our RNAseq data, including *MKI67* and *CDK1*, indicating that
269 migrated hiPSC-CMs were more proliferative than their non-migrated counterparts. This
270 observed difference could be a potential advantage when transplanting hiPSC-CMs *in vivo*. As
271 we aim to improve the intra-cardiac migration of donor hiPSC-CMs, their potential increase in
272 proliferation could further contribute to the remuscularisation of the heart after their migration
273 into the infarcted tissue. Further study is warranted to confirm and regulate the proliferative
274 profile of migrated cells.

275 In this study, we also explored the relationship between maturation of hiPSC-CM and their
276 migration ability. Over prolonged culture, hiPSC-CM migration ability either remained
277 unchanged or diminished, depending on the cell line. Whilst the migration percentage of
278 hiPSC-CM-A towards LV homogenate remained around 20-30% up to day 45 of
279 differentiation, the migration ability of hiPSC-CM-B decreased from 31% (day 15) to 9% (day
280 45). Further detailed analysis of these cell lines at different stages of maturation is required to
281 determine the optimal stage of differentiation for transplantation. Apart from shifts in their
282 maturation phase and migration ability, these cell lines are likely to experience alterations in

283 other characteristics (e.g. metabolic profile, sensitivity to hypoxia or inflammation) during
284 various stages that could impact their suitability for transplantation.

285 Furthermore, in this study we observed the typical early expression of the atrial associated
286 marker MLC2a, which decreased over time whilst the percentage of ventricular MLC2v-
287 positive cells increased with time. This needs to be considered when designing cell-based
288 therapies for heart failure and raises the question whether the migration mechanism is
289 substantially different for different subtypes of hiPSC-CMs. However, no major differences in
290 *MYL2* (MLC2a) or *MYL7* (MLC2v) expression were observed between the migrated and non-
291 migrated groups, indicating that both subtypes (and double positive cells) have the capability
292 to migrate towards an MI stimulus. Recently, protocols that generate near-homogenous LV
293 CMs from hiPSCs have been published[42], and commercial kits generating only ventricular
294 hiPSC-CMs have become available (STEMCELL Technologies). Future studies using highly
295 pure populations of LV hiPSC-CMs in our migration assays would shed light on the influence
296 of CM subtype on migration ability and/or mechanism.

297 In summary, our findings reveal new insights into the migratory abilities of hiPSC-CMs and
298 shed light on the complex mechanisms that drive their movement in response to an ischaemic
299 post-MI stimulus. These discoveries offer clarity for enhancing treatments aimed at cardiac
300 regeneration, and hold promise for potentially achieving substantial scientific and clinical
301 impact in stem cell and cardiovascular research.

Bibliography

1. Tsao, C. W. *et al.* Heart Disease and Stroke Statistics—2023 Update: A Report From the American Heart Association. *Circulation* **147**, E93–E621 (2023).

2. Kormos, R. L. *et al.* The Society of Thoracic Surgeons Intermacs Database Annual Report: Evolving Indications, Outcomes, and Scientific Partnerships. *Ann Thorac Surg* **107**, 341–353 (2019).

3. Slaughter, M. S. *et al.* Advanced heart failure treated with continuous-flow left ventricular assist device. *New England Journal of Medicine* **361**, 2241–2251 (2009).

4. Kawamura, T. *et al.* Safety confirmation of induced pluripotent stem cell-derived cardiomyocyte patch transplantation for ischemic cardiomyopathy: first three case reports. *Front Cardiovasc Med* **10**, 1–9 (2023).

5. Shiba, Y. *et al.* Allogeneic transplantation of iPS cell-derived cardiomyocytes regenerates primate hearts. *Nature* **538**, 388–391 (2016).

6. Safety and Efficacy of Induced Pluripotent Stem Cell-derived Engineered Human Myocardium as Biological Ventricular Assist Tissue in Terminal Heart Failure. ClinicalTrials.gov identifier: NCT04396899. Updated March 27, 2023. Accessed February 06,2025. https://clinicaltrials.gov/study/NCT04396899

7. Miki, K. *et al.* Bioengineered Myocardium Derived from Induced Pluripotent Stem Cells Improves Cardiac Function and Attenuates Cardiac Remodeling Following Chronic Myocardial Infarction in Rats. *Stem Cells Transl Med* **1**, 430–437 (2012).

8. Hata, H. *et al.* Engineering a novel three-dimensional contractile myocardial patch with cell sheets and decellularised matrix. *European Journal of Cardio-thoracic Surgery* **38**, 450–455 (2010).

9. Moyes, K. W. *et al.* Human Embryonic Stem Cell-Derived Cardiomyocytes Migrate in Response to Gradients of Fibronectin and Wnt5a. *Stem Cells Dev* **22**, 2315–2325 (2013).

10. Wilson, K. D. *et al.* Endogenous Retrovirus-Derived lncRNA BANCR Promotes Cardiomyocyte Migration in Humans and Non-human Primates. *Dev Cell* **54**, 694-709.e9 (2020).

11. Hosen, M. R. *et al.* Airn Regulates Igf2bp2 Translation in Cardiomyocytes. *Circ Res* **122**, 1347–1353 (2018).

12. Qin, X., Gao, S., Yang, Y., Wu, L. & Wang, L. microRNA-25 promotes cardiomyocytes proliferation and migration via targeting Bim. *J Cell Physiol* **234**, 22103–22115 (2019).

13. Bergeron, A. *et al.* Filamentous nestin and nonmuscle myosin IIB are associated with a migratory phenotype in neonatal rat cardiomyocytes. *J Cell Physiol* **236**, 1281–1294 (2021).

14. Bock-Marquette, I., Saxena, A., White, M. D., DiMaio, J. M. & Srivastava, D. Thymosin β4 activates integrin-linked kinase and promotes cardiac cell migration, survival and cardiac repair. *Nature* **432**, 466–472 (2004).

15. Chablais, F. & Jaźwińska, A. The regenerative capacity of the zebrafish heart is dependent on TGFβ signaling. *Development* **139**, 1921–1930 (2012).

16. Peng, Y. *et al.* Inhibition of TGF-β/Smad3 Signaling Disrupts Cardiomyocyte Cell Cycle Progression and Epithelial–Mesenchymal Transition-Like Response During Ventricle Regeneration. *Front Cell Dev Biol* **9**, 1–14 (2021).

17. Itou, J. *et al.* Migration of cardiomyocytes is essential for heart regeneration in zebrafish. *Development (Cambridge)* **139**, 4133–4142 (2012).

18. Burridge, P. W., Holmström, A. & Wu, J. C. Chemically Defined Culture and Cardiomyocyte Differentiation of Human Pluripotent Stem Cells. *Curr Protoc Hum Genet* **87**, 21.3.1-21.3.15 (2015).

19. Burridge, P. W. *et al.* Chemically defined generation of human cardiomyocytes. *Nat Methods* **11**, 855–860 (2014).

20. Lundy, S. D., Zhu, W. Z., Regnier, M. & Laflamme, M. A. Structural and functional maturation of cardiomyocytes derived from human pluripotent stem cells. *Stem Cells Dev* **22**, 1991–2002 (2013).

21. Zuppinger, C. *et al.* Characterization of cytoskeleton features and maturation status of cultured human iPSC-derived cardiomyocytes. *European Journal of Histochemistry* **61**, 145–153 (2017).

22. Ormrod, B. & Ehler, E. Induced pluripotent stem cell-derived cardiomyocytes—more show than substance? *Biophys Rev* **15**, 1941–1950 (2023).

23. Cappelli, C. *et al.* The TGF-β profibrotic cascade targets ecto-5'-nucleotidase gene in proximal tubule epithelial cells and is a traceable marker of progressive diabetic kidney disease. *Biochim Biophys Acta Mol Basis Dis* **1866**, 165796 (2020).

24. Dituri, F., Cossu, C., Mancarella, S. & Giannelli, G. The Interactivity between TGFβ and BMP Signaling in Organogenesis, Fibrosis, and Cancer Activated Protein Kinases (MAPKs, namely Extracellular Receptor Kinase 1 and 2-ERK1/2. *Cells* **8**, 1–21 (2019).

25. Hou, J. *et al.* DACT2 regulates structural and electrical atrial remodeling in atrial fibrillation. *J Thorac Dis* **12**, 2039–2048 (2020).

26. Kramerova, I. *et al.* Spp1 (osteopontin) promotes TGFβ processing in fibroblasts of dystrophin-deficient muscles through matrix metalloproteinases. *Hum Mol Genet* **28**, 3431 (2019).

27. Lange, A. W., Keiser, A. R., Wells, J. M., Zorn, A. M. & Whitsett, J. A. Sox17 promotes cell cycle progression and inhibits TGF-β/Smad3 signaling to initiate progenitor cell behavior in the respiratory epithelium. *PLoS One* **4**, (2009).

28. Thuault, S. *et al.* Transforming growth factor-β employs HMGA2 to elicit epithelial-mesenchymal transition. *Journal of Cell Biology* **174**, 175–183 (2006).

29. Li, Q., Xu, Y., Li, X., Guo, Y. & Liu, G. Inhibition of Rho-kinase ameliorates myocardial remodeling and fibrosis in pressure overload and myocardial infarction: Role of TGF-β1-TAK1. *Toxicol Lett* **211**, 91–97 (2012).

30. Vilahur, G. *et al.* Molecular and cellular mechanisms involved in cardiac remodeling after acute myocardial infarction. *J Mol Cell Cardiol* **50**, 522–533 (2011).

31. Inman, G. J. *et al.* SB-431542 is a potent and specific inhibitor of transforming growth factor-β superfamily type I activin receptor-like kinase (ALK) receptors ALK4, ALK5, and ALK7. *Mol Pharmacol* **62**, 65–74 (2002).

32. Reibman, J. *et al.* Transforming growth factor β1, a potent chemoattractant for human neutrophils, bypasses classic signal-transduction pathways. *Proc Natl Acad Sci U S A* **88**, 6805–6809 (1991).

33. Wahl, S. M. *et al.* Transforming growth factor type β induces monocyte chemotaxis and growth factor production. *Proc Natl Acad Sci U S A* **84**, 5788–5792 (1987).

34. Liu, Z., Yi, L., Du, M., Gong, G. & Zhu, Y. Overexpression of TGF-β enhances the migration and invasive ability of ectopic endometrial cells via ERK/MAPK signaling pathway. *Exp Ther Med* 4457–4464 (2019) doi:10.3892/etm.2019.7522.

35. Melzer, C., von der Ohe, J., Hass, R. & Ungefroren, H. TGF-β-dependent growth arrest and cell migration in benign and malignant breast epithelial cells are antagonistically controlled by Rac1 and Rac1b. *Int J Mol Sci* **18**, (2017).

36. Zhao, W. *et al.* Effect of TGF-β1 on the Migration and Recruitment of Mesenchymal Stem Cells after Vascular Balloon Injury: Involvement of Matrix Metalloproteinase-14. *Sci Rep* **6**, 1–11 (2016).

37. Azhar, M. *et al.* Transforming growth factor beta in cardiovascular development and function. *Cytokine Growth Factor Rev* **14**, 391–407 (2003).

38. Hanna, A. & Frangogiannis, N. G. The Role of the TGF-β Superfamily in Myocardial Infarction. *Front Cardiovasc Med* **6**, 1–15 (2019).

39. Dobaczewski, M., Gonzalez-Quesada, C. & Frangogiannis, N. G. The extracellular matrix as a modulator of the inflammatory and reparative response following myocardial infarction. *Journal of Molecular and Cellular Cardiology* Preprint at https://doi.org/10.1016/j.yjmcc.2009.07.015 (2010).

40. Yi, X. *et al.* Hepatocyte growth factor regulates the TGF-β1-induced proliferation, differentiation and secretory function of cardiac fibroblasts. *Int J Mol Med* **34**, 381–390 (2014).

41. Pardali, E. & Dijke, P. Transforming growth factor-beta signalling and tumor angiogenesis. *Mol Cell* **14**, 4848–4861 (2009).

42. Dark, N. *et al.* Generation of left ventricle-like cardiomyocytes with improved structural, functional, and metabolic maturity from human pluripotent stem cells. *Cell Reports Methods* **3**, 100456 (2023).

412 **METHODS AND MATERIALS**

413 ***Human iPSC culture***

414 Four hiPSC lines were obtained from the European Bank for Induced Pluripotent Stem Cells
415 (EBiSC) and cultured in feeder-free, serum-free 2D culture at 37°C and 5% CO_2. For the
416 generation of hiPSC-CMs, the differentiation method was based on the protocol published by
417 Burridge et al.[18]. Briefly, hiPSCs were grown in E8 Flex medium (Thermofisher) on
418 recombinant human vitronectin (rhVTN)-coated plates for 3-4 days until reaching ~85%
419 confluency. Differentiation was initiated by incubating the cells in CDM3 medium (RPMI 1640
420 + 75 mg/mL recombinant human albumin (Merck) + 64 mg/mL L-ascorbic acid 2-phosphate
421 (Merck) supplemented with 6 μM CHIR99021 (Cambridge Bioscience). After two days, the
422 medium was replaced with CDM3 supplemented with 2 μM Wnt-c59. After, the cell media was
423 refreshed with CDM3 medium every 2 days. Alternatively, hiPSC-CMs were generated with
424 the commercial CM Differentiation Kit by STEMCELL Technologies where indicated.

425

426 ***Heart tissue homogenisation***

427 Adult male Sprague-Dawley rats underwent LCA ligation to induce MI or sham surgery. For
428 MI, the left coronary artery was ligated at the level of the bottom edge of the left atrial
429 appendage through left thoracotomy under isoflurane anaesthesia and mechanical ventilation.
430 Ischemia was confirmed by a change in the epicardial colour and dyskinesis. The rats were
431 returned to the cage for recovery after chest and skin closure and extubation. The sham group
432 received an open/close chest procedure. The rats were sacrificed after 1 day, after which the
433 LV wall was harvested. The tissue samples were then either freshly homogenised or snap frozen
434 in liquid nitrogen and stored at -80°C until further use. The tissue samples were homogenised
435 in PBS supplemented with protease inhibitors (cOmplete, EDTA-free Protease Inhibitor

436 Cocktail, Sigma-Aldrich) in a Precellys 24 tissue homogeniser. The homogenised samples were
437 centrifuged for 15 mins at 6000 g and the supernatant was collected for immediate use or stored
438 at -80°C.

439 All procedures on living animals were performed with the approval of the institutional ethics
440 committee at Queen Mary University of London and the Home Office, UK. The investigation
441 conforms to the Principles of Laboratory Animal Care formulated by the National Society for
442 Medical Research and the Guide for the Care and Use of Laboratory Animals (US National
443 Institutes of Health Publication, 1996).

444

445 ***Wound healing assay***

446 HiPSC-CMs were seeded at a density of ≥ 2.5 x 10^5 cells/cm^2 to form a confluent monolayer
447 and incubated with 10 µM Y-27632, Rock inhibitor (Cambridge BioScience) overnight to allow
448 cell attachment. A scratch wound was made with a P1000 tip and following a wash with PBS,
449 hiPSC-CMs were incubated with either cell media alone or supplemented with a dilution of left
450 ventricle homogenate of an MI or sham rat heart for up to 24 hours. To assess migration, images
451 were captured with a Keyence BZ-X810 microscope or an EVOS XL Core Cell Imaging
452 System. ImageJ software was used to measure the percentage of wound closure and cell front
453 migration. For the percentage of wound closure, the difference in wound area between the
454 timepoint of interest and the initial wound area (μm^2) is measured and divided over the initial
455 wound area (μm^2) and multiplied x 100. For front cell migration, the difference in wound area
456 between the timepoint of interest and initial wound area (μm^2) is divided by the height of the
457 image (µm), which represents the y-axis, to obtain the difference in horizontal distance (x-axis),
458 i.e., the cell front migration (µm). This number is then divided by the incubation time to obtain
459 the cell front migration speed.

460 ***Transwell migration assay***

461 All TWM assays were performed in 24-well plates. Prior to seeding, 24-well inserts (8 μM,
462 Starstedt) were coated on both sides with ~22 μg/cm^2 Geltrex Ready to Use (Thermofisher) for
463 1h at 37°C. After aspiration of the remaining liquid, 1 x 10^5 hiPSC-CMs were seeded in
464 cardiomyocyte support medium supplemented with 10 μM Y-27632, Rock inhibitor in the
465 upper compartment overnight to allow cell attachment. The next day, the media was replaced
466 and cell medium alone or containing a dilution of left ventricle homogenate of an MI rat heart
467 was added to the lower compartment. Migration was assessed by fixation of the membrane in
468 4% paraformaldehyde for 15 mins at room temperature (RT) followed by a washing step in
469 PBS and incubation with DAPI for 15 mins at RT. To visualise migrated cells only, the upper
470 part of the insert was swabbed with a cotton swab. The membranes were removed and mounted
471 on microscopic slides for visualisation. Images were acquired on a Keyence BZ-X180 or Zeiss
472 LSM800 microscope. Quantification was performed using ImageJ.

473

474 ***ELISA***

475 TGF-β1 levels were measured in sham and MI homogenate using a TGF-beta 1 Quantikine
476 ELISA kit (R&D, DB100C). Latent TGF-β1 was activated by incubation of the supernatant
477 with 1M HCl for 10 mins, followed by neutralisation with 1.2M NaOH/0.5M HEPES. Next,
478 Assay Diluent was added to each well of a provided TGF-β1 microplate, followed by standard
479 or activated sample. After 2h of incubation, the plate was washed four times before a 2h
480 incubation with TGF-β1 conjugate. After four additional washes, substrate solution was added
481 to each well and incubated for 30 mins. Then, stop solution was added to each well and the
482 optical density of each well was measured with a microplate reader set to 450 nm with
483 wavelength correction of 540 nm.

484 ***Bulk RNAseq***

485 HiPSC-CMs were seeded at day 15 of differentiation on transwell inserts as described above.
486 After 24 hours of incubation with a 1:10 dilution of left ventricle homogenate of an MI rat heart
487 in the lower compartment, all culture media was aspirated from the inserts followed by a wash
488 step with PBS. The transwell inserts were then swabbed on either the upper side or lower side
489 of the insert, to collect the migrating or non-migrating cells respectively. RNA extraction was
490 performed by incubating the inserts directly in RLT lysis buffer of the Qiagen RNeasy mini kit
491 and the manufacturer's protocol was then followed accordingly. A minimum of 100 ng of RNA
492 was used with RIN values ≥ 9.4 for bulk RNAseq (20M reads). Illumina PE150 next generation
493 sequencing and data analysis was carried out by Novogene Ltd.

494

495 ***Immunocytochemistry***

496 HiPSCs were harvested by incubation with EDTA for 3-5 mins followed by aspiration and
497 detachment with culture media, and subsequently seeded onto 16 mm coverslips in 12 well
498 plates coated with rhVTN and cultured for 2-4 days before fixation with 4%
499 paraformaldehyde/PBS for 15 min at 37°C.

500 HiPSC-CMs were replated overnight using the CM dissociation kit (Thermofisher) before
501 fixation. In short, wells were 2x washed with PBS before incubation with cardiomyocyte
502 dissociation medium at 37°C for 10-15 mins. Cells were dislodged by resuspension with a 10
503 mL serological pipette and transferred to a tube containing cardiomyocyte support medium.
504 After centrifugation at 300 g for 5 min, the supernatant was discarded, and the pellet was
505 resuspended in cardiomyocyte support medium supplemented with 5 µM Y-27632 and seeded
506 into a new rhVTN-coated plate at the desired density (≥ 2.5 x 10^5 cells/cm^2) overnight. The
507 next day, the hiPSC-CMs were fixed with 4% paraformaldehyde/PBS for 15 mins at 37°C.

508 HiPSCs/hiPSC-CMs were subsequently washed and permeabilised with 0.1% Triton-X-
509 100/PBS for 10 min at RT and blocked using 10% donkey serum/PBS for 1h at RT. Cells were
510 stained with primary antibodies overnight at 4°C in the dark, washed and stained with
511 secondary antibodies for 30 mins at 37°C. The antibodies used can be found in Supplementary
512 Table S4-5. After a subsequent washing step, cells were counterstained with DAPI. Washing
513 steps were performed with 0.1% Tween:PBS. Cell samples were imaged with a Zeiss LSM 800
514 or Keyence BZ-X810 microscope.

515

516 ***Flow cytometry***

517 HiPSCs were harvested by incubation with EDTA for 3-5 mins followed by aspiration and
518 detachment with culture media. Cells were then transferred to 15 mL tubes and centrifuged at
519 200 g for 5 mins. The supernatant was aspirated, and cells were resuspended into single cells
520 in filtered FACS buffer (PBS, 4% w/v bovine serum albumin (BSA), 10% v/v Penicillin-
521 Streptomycin (Pen-Strep), 4% v/v EDTA). After repeating the last step, the cells were stained
522 for 30 mins at RT. The antibodies used can be found in Supplementary Table S4-5.

523

524 HiPSC-CMs were dissociated with the Cardiomyocyte Dissociation Kit (see above) and stained
525 with the Inside Stain Kit (Miltenyi Biotech) according to the manufacturer's protocol. Briefly,
526 dissociated cells are counted with Trypan Blue and up to 1 million cells are washed by adding
527 FACS buffer. After centrifugation at 200 g for 10 mins, the cells are resuspended in 1:1 FACS
528 buffer/Inside Fix buffer. After 20 mins of incubation in the dark at RT, the cells are washed
529 with FACS buffer and centrifuged at 200 g for 5 mins. The washing step is repeated in Inside
530 Perm. The cells were directly stained in Inside Perm buffer for 10-30 mins at RT, or indirectly
531 for 1h at RT and with secondary antibodies for 30 mins at RT in the dark. The antibodies used
532 can be found in Supplementary Table S4-5.

533 HiPSCs/hiPSC-CMs were subsequently washed and resuspended in incubation medium and
534 were kept on ice until analysis. Data was acquired on a BD LSRFortessa instrument and
535 analysed using FlowJo software.
536
537 ***Real-time quantitative PCR (RT-qPCR)***
538 Total RNA isolation was performed using the RNeasy mini kit (Qiagen) according to the
539 manufacturer's protocol. Briefly, harvested cells or heart homogenates were lysed in RLT lysis
540 buffer for 5 mins at RT. The resulting cell lysate was transferred to a QIAShredder column and
541 was centrifuged at full speed for 3 mins. Next, 70% ethanol was added to the lysate, which was
542 transferred to an RNeasy silica column, followed by centrifugation at 1.2 x 10^4 rpm for 15s.
543 This was followed by a washing step in RW1 wash buffer and a DNase I incubation for 15 mins
544 at RT, followed by another wash step with RW1 and twice with RPE, followed by dry
545 centrifugation of the column at 1.2 x 10^4 rpm for 1 min. The RNA was eluted in RNase free
546 ddH2O for 2 min at RT followed by centrifugation at 1.2 x 10^4 rpm for 1 min. Eluted RNA was
547 kept on ice until further use or stored at -80°C for future use. RNA was subsequently reverse
548 transcribed into cDNA with the High Capacity Reverse Transcription Kit (Thermofisher,
549 4368814) with the following thermal cycler settings: 10 min at 25°C, 120 mins at 37°C, 5 mins
550 at 85°C. Gene expression was quantified by real-time PCR of 10 ng cDNA of each sample with
551 the PowerUp SYBR Green supermix (Thermofisher, A257420). Primers for each gene are
552 given in Table S6. β-actin and GAPDH were used as housekeeping genes. Of note, the use of
553 β-actin and GAPDH as reference genes has been critiqued as these genes show variable levels
554 of expression in different tissues during development including the heart, which might
555 compromise their role in gene expression normalisation (Lin & Redies, 2012).

556 The plate was transferred to a QuantStudio 7.0 Real-Time PCR machine (Applied Biosystems)
557 and the following parameters were applied: 5 mins 95°C, 40 cycles of 15s at 95°C, 30s at 60°C
558 and 30s at 72°C, followed by a melt curve analysis from 55-95°C.
559
560 ***Statistics***

561 All data was analysed using Graphpad Prism 9.0 software (Graphpad, San Diego, CA). Data is
562 represented as mean ± standard deviation (SD). Statistical analysis was performed on data with
563 a replicate number of 3 and above. Technical replicates are indicated with 'n' and biological
564 replication with 'N', as detailed in the figure legends. For the comparison between two groups,
565 two-tailed unpaired Student's t-tests were performed. Multiple group comparisons were
566 performed with one-way or two-way analysis of variance (ANOVA) with Tukey's post hoc test
567 correction (3 groups) or Dunnett's correction (>3 groups). If the number of replicates was not
568 equal between groups, a mixed-effects analysis was performed instead of an ANOVA, as the
569 latter cannot deal with missing values. Statistical significance was accepted at $p < 0.05$.

570

571 **AUTHOR CONTRIBUTIONS**

572 KS, FLM and LD conceived and designed the study. LD performed the majority of the
573 experiments. KK and AHAG contributed to the execution of select experiments. LD, KS and
574 FLM analysed the data and wrote the manuscript. All the authors read and approved the
575 manuscript.

576

577 **COMPETING INTERESTS STATEMENT**

578 The authors declare that they have no competing financial interests.

Figure 1

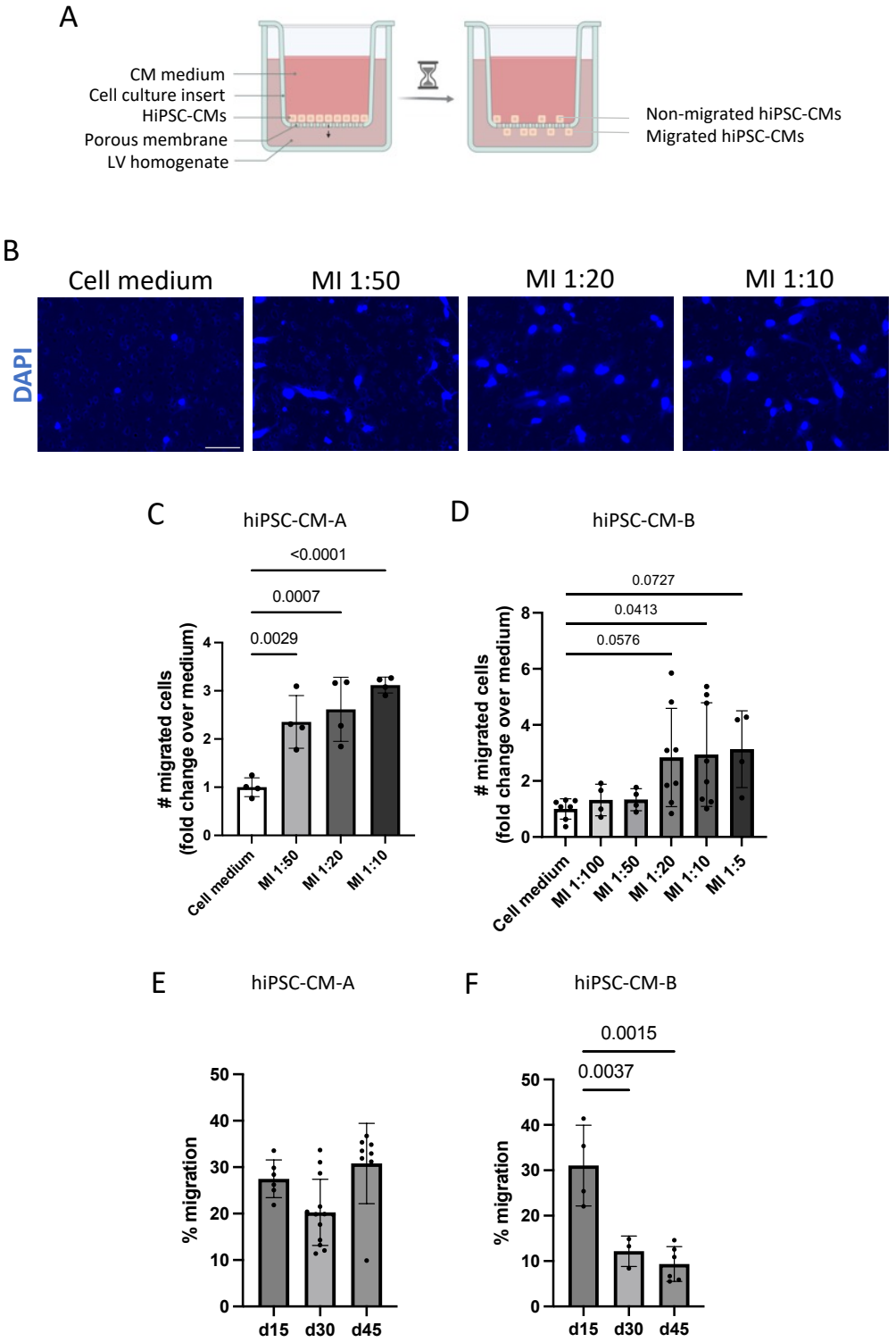

FIG 1. Human iPSC-CMs show a concentration-dependent chemotactic response to an MI stimulus that varies with maturation stage. A) Schematic of the transwell migration assay. B-D) HiPSC-CMs were seeded at day 15 and fixed and stained at 24h after incubation with cell medium, non-MI or MI homogenate at different dilutions. Non-migrated hiPSC-CMs on the top of the membrane were swabbed away and migrated hiPSC-CMs were imaged. B-C) hiPSC-CM-A, n=4. DAPI staining was used to visualise nuclei. Scale bar: 50 µm. D) hiPSC-CM-B, n=4-8, N=2. E-F) hiPSC-CM-A and hiPSC-CM-B were seeded at different days of differentiation and fixed and stained at 24h after incubation with MI homogenate (1:10), n= 6-10, N=1-3 (E), n=3-6, N=1-2 (F). Technical replicates are indicated with 'n' and biological replication with 'N'. Statistical analyses were performed using one-way ANOVA with Dunnett's correction. Error bars indicate mean ± SD.

Figure 2

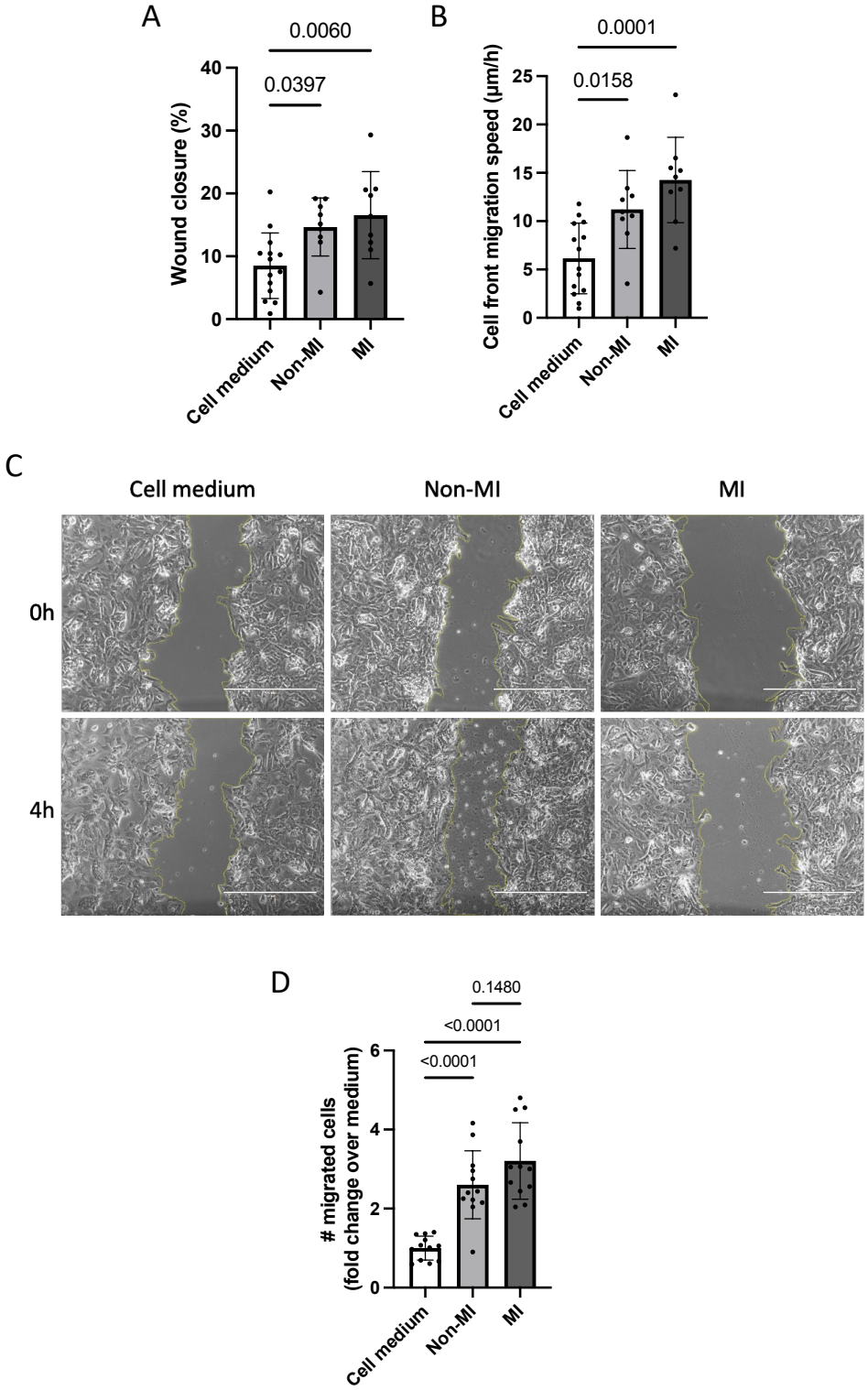

FIG 2. Human iPSC-CMs show a two-fold increase in migration when exposed to an MI environment. A-C) Day 15 hiPSC-CM-D (commercial kit) were replated to form a monolayer and a scratch was generated. HiPSC-CM-D were incubated with cell medium only (n=14) or supplemented with MI (1:10, n=9) or non-MI homogenate (1:10, n=9), wound closure (A) and cell front migration speed (B) were measured after 4h of incubation, N=2. C) Representative images of day 15 hiPSC-CM-D in the scratch wound assay. Scale bar: 1000 µm. D) Day 15 hiPSC-CM-A were seeded on transwell inserts and exposed to a 1:20 dilution of MI or non-MI homogenate for 4h (n=12). Technical replicates are indicated with 'n' and biological replication with 'N'. Statistical analyses were performed using a one-way ANOVA followed by Tukey's pairwise comparisons. Error bars indicate mean ± SD.

Figure 3

A

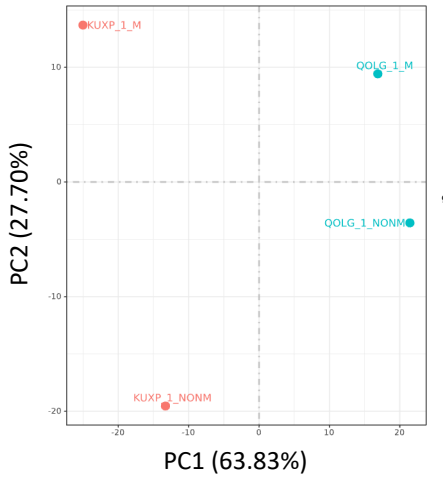

C

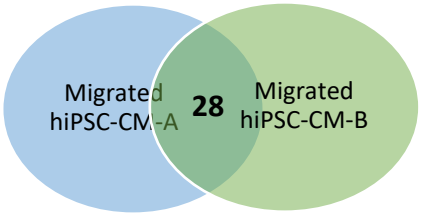

D

PTX3	SOX17	BMP6	TGFBI	SPP1
NTM	GLIPR1	VIPR1	RGPD6	NT5E
CASP4	OAS3	F2RL2	BGN	CLMP
EPAS1	NFE2L3	KCNJ2	KIF18B	MKI67
HMGA2	VEPH1	F2RL3	CDK1	SLC7A11
DACT2	NEK2	DHRS2		

B

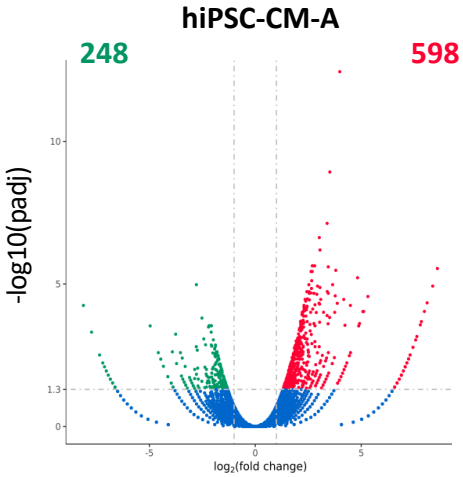

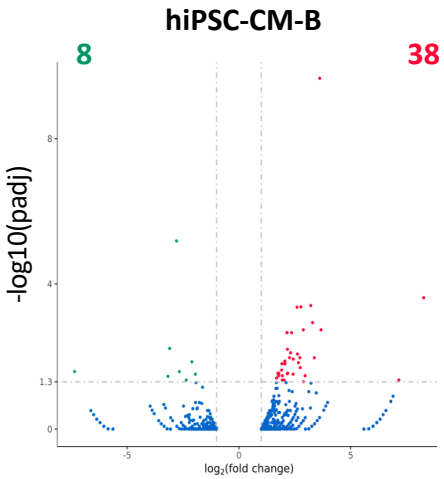

E

Cellular and molecular functions associated with hiPSC-CM migration	
hiPSC-CM-A	
Cellular and molecular function	P-value range
Cell Cycle	4.77E-11 – 1.64E-29
Cellular Assembly and Organization	4.60E-11 – 1.64E-29
DNA Replication, Recombination, and Repair	4.60E-11 – 1.64E-29
Cellular Movement	2.47E-11 – 2.69E-23
Cell Death and Survival	6.70E-12 – 8.52E-23
hiPSC-CM-B	
Cellular and molecular function	P-value range
Cellular Development	1.21E-03 – 3.45E-08
Cell Cycle	8.86E-04 – 8.79E-08
Cell Death and Survival	1.03E-03 – 3.17E-07
Cellular Movement	1.34E-03 – 3.53E-07
Cell Morphology	1.37E-03 – 6.22E-07

FIG 3. Migrated and non-migrated hiPSC-CMs represent distinct populations after 24h of incubation with MI homogenate. HiPSC-CM-A and hiPSC-CM-B were seeded on transwell inserts at day 15. After incubation overnight, the hiPSC-CMs were exposed to a 1:10 dilution of MI homogenate for 24h. Subsequently, migrated and non-migrated cells were harvested separately and analysed by bulk RNAseq. A) PCA plot. B) Differentially expressed genes in migrated cells versus non-migrated cells in hiPSC-CM-A and hiPSC-CM-B after 24h. Red dots indicate significantly upregulated genes, green dots indicate significantly downregulated genes and blue dots indicate genes which are not significantly differentially expressed. The cut-off parameters were chosen as log2FoldChange > |1| and padj or false discovery rate (FDR) <0.05. C-D) Combining the datasets resulted in a panel of 28 shared genes. E) Cellular and molecular functions associated with hiPSC-CM migration generated from the 24h dataset via Ingenuity Pathway Analysis.

Figure 4

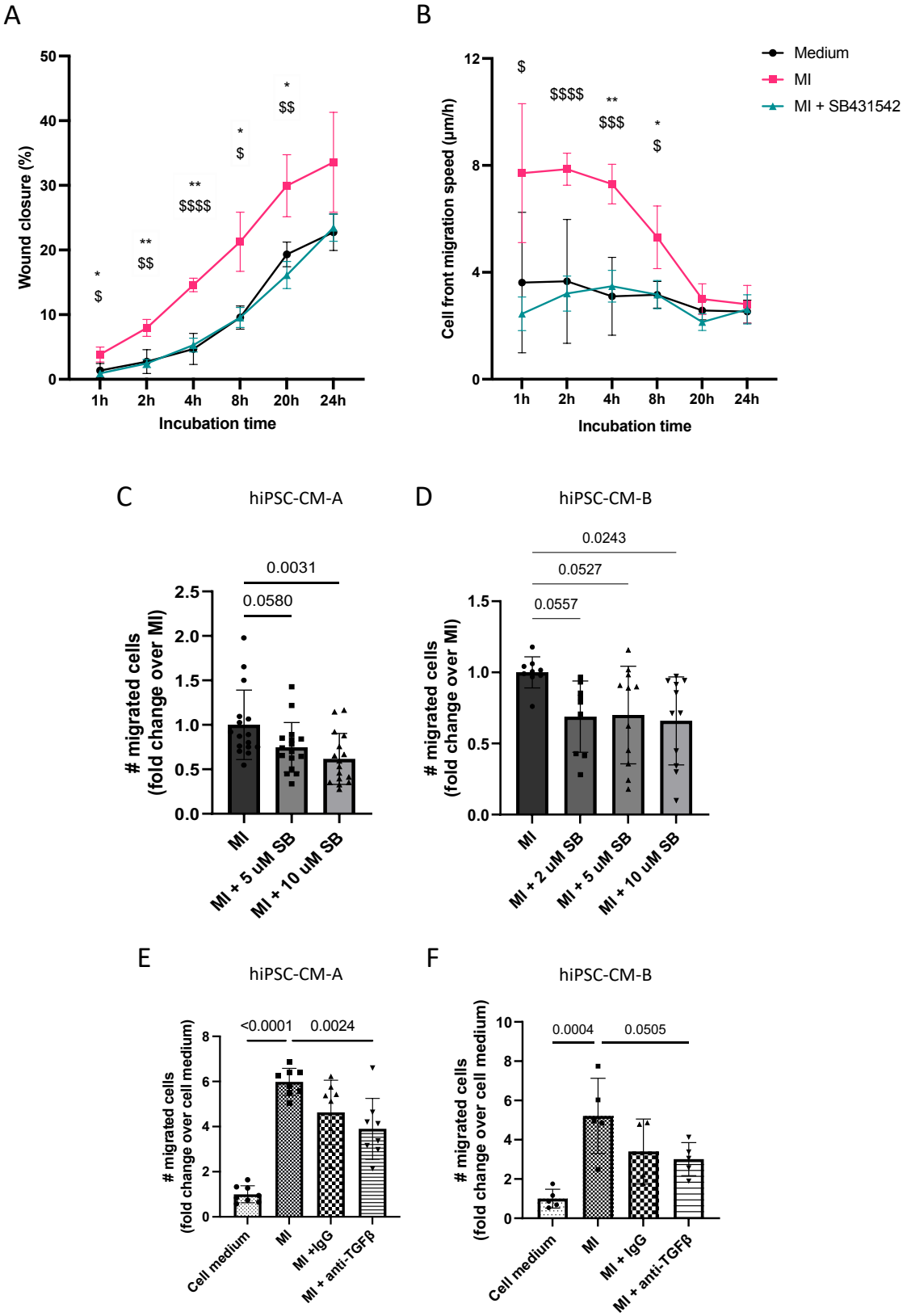

FIG 4. Inhibiting TGF-β signalling decreases MI-induced hiPSC-CM migration. A-B) Day 15 hiPSC-CM-A were seeded overnight and incubated with medium, MI 1:20 or MI 1:20 supplemented with 10 µM SB431542, n=4. *: P<0.05, **: P<0.01, MI vs. medium, $: P<0.05, $$: P<0.01, $$$: P<0.001, $$$$: P<0.0001, MI vs. MI + SB431542. C-D) HiPSC-CMs were seeded on transwell inserts and exposed to MI 1:20 only or with a 15-minute pre-incubation of 5 µM or 10 µM SB431542 prior to incubation with MI for 4h. C) hiPSC-CM-A, N=2 (d15 and d16), n=16. D) hiPSC-CM-B, N=3 (d15), n=10-11. E-F) D15 hiPSC-CMs were seeded on transwell inserts and exposed to cell medium, MI 1:20 only or MI with 20 ng/mL IgG or TGF-β neutralisation antibody for 4h. E) hiPSC-CM-A, n=12. F) hiPSC-CM-B, n=4-5. Technical replicates are indicated with 'n' and biological replication with 'N'. Statistical analyses were performed using a one-way ANOVA followed by Tukey's pairwise comparisons (C) or Dunnett's correction (D-F). Error bars indicate mean ± SD.

Figure S1

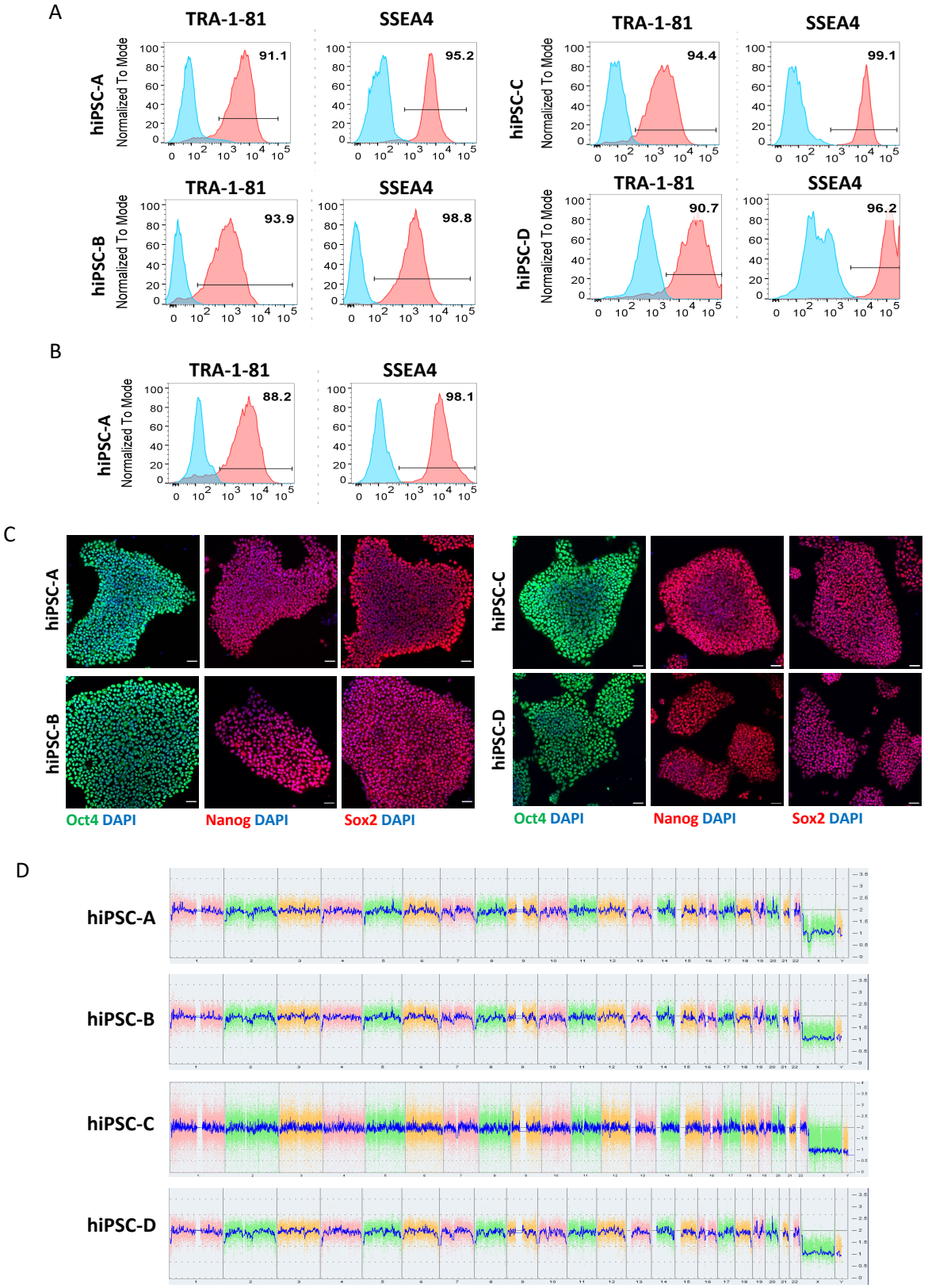

FIG S1: Pluripotency and karyotype normality of hiPSC lines. A) Flow cytometric analysis of pluripotency markers, TRA-1-81 and SSEA4 of hiPSC-A (P47), hiPSC-B (P34), hiPSC-C (P34) and hiPSC-D (P41). Samples are shown in red and isotype controls are shown in blue. B) Flow cytometric analysis of TRA-1-81 and SSEA4 of hiPSC-A at passage 77. C) Representative micrographs showing immunolabelling of pluripotency markers Oct-4 (green), Nanog (red) and Sox2 (red), nuclei are labelled with DAPI (blue). Scalebar: 50 µm. D) hiPSCs A-D were negative for karyotypic abnormalities confirmed by KaryoStat analysis at passage 54, 47, 36 and 44, respectively. The whole genome view displays all somatic and sex chromosomes in one frame with copy number levels. The pink, green and yellow colours indicate the raw signal for each individual chromosome probe, while the blue signal represents the normalized probe signal which is used to identify copy number and potential aberrations deviating from a normal copy number state (CN = 2).

Figure S2

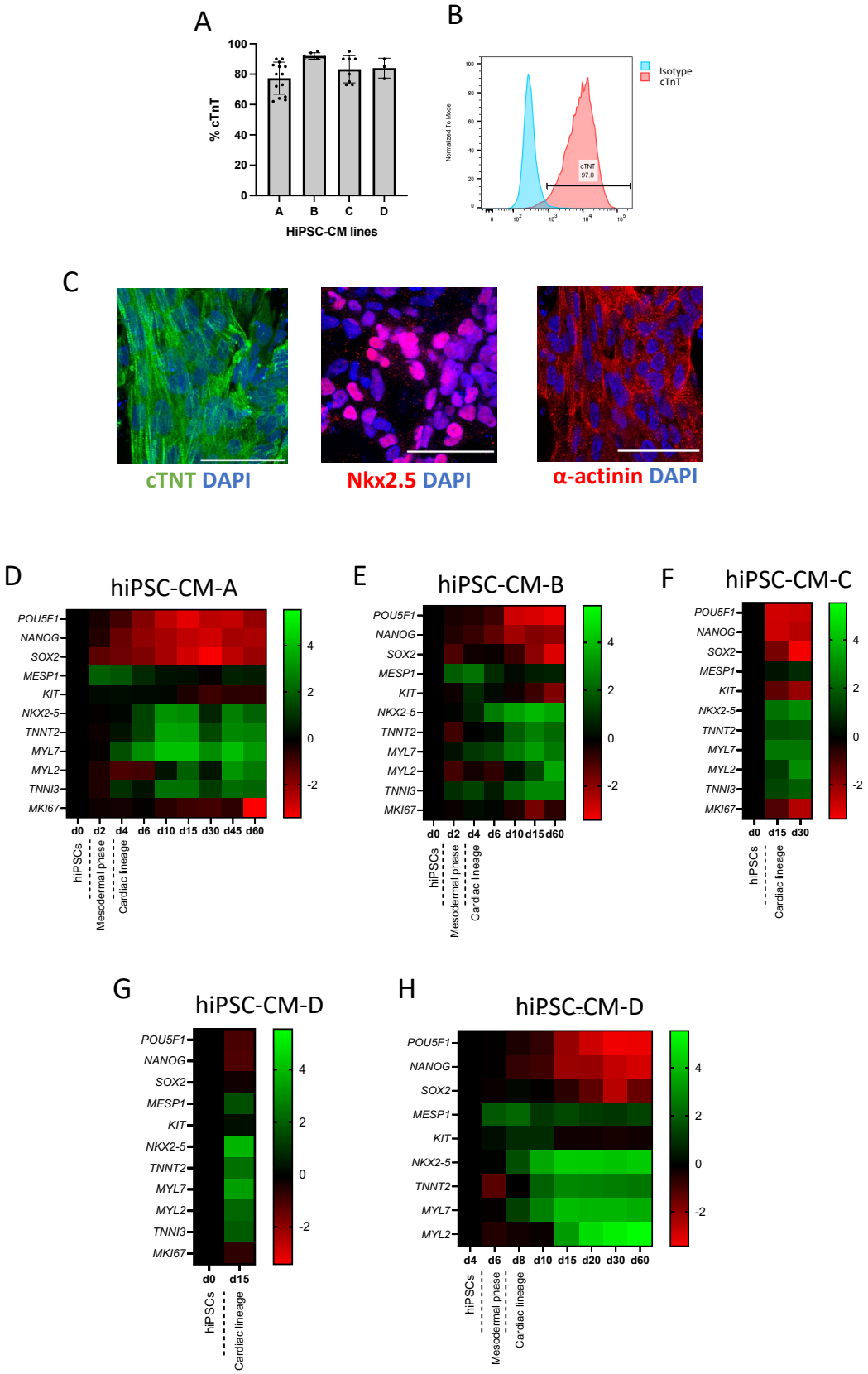

FIG S2: Expression of pluripotency and cardiac markers during hiPSC-CM differentiation using the Burridge protocol and commercial kit. A) Differentiation efficiency measured by cTnT expression in hiPSC-CM-A-D lines using the Burridge et al. protocol. B) Representative graph of cTnT expression measured in hiPSC-CM-B at day 15. C) Representative micrographs showing immunolabelling for cardiac markers at day 0 and 15 of hiPSC-CM-D differentiation using the commercial kit. Scalebar: 50 µm. D-H). Heat maps illustrating quantitative RT-qPCR analysis of pluripotent, mesodermal, and cardiac marker expression during hiPSC-CM differentiation of hiPSC-CM-A (D), hiPSC-CM-B (E), hiPSC-CM-C (F) and hiPSC-CM-D (G) using the Burridge protocol and hiPSC-CM-D using the commercial kit (H). Values are represented as log fold change and represent the average of 1-3 samples.

Figure S3

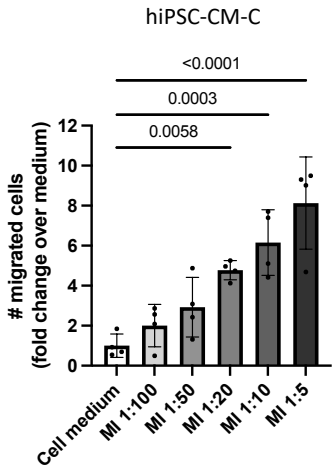

Fig S3: MI homogenate has a concentration-dependent effect on hiPSC-CM-C migration. HiPSC-CM-C were seeded onto transwells at day 15 and fixed and stained at 24h after incubation with cell medium, non-MI or MI homogenate at different dilutions. Non-migrated hiPSC-CMs on the top of the membrane were swabbed away and migrated hiPSC-CMs were imaged. n=4. Statistical analysis was performed using one-way ANOVA followed by Dunnett's correction. Error bars indicate mean $\pm$ SD.

Figure S4

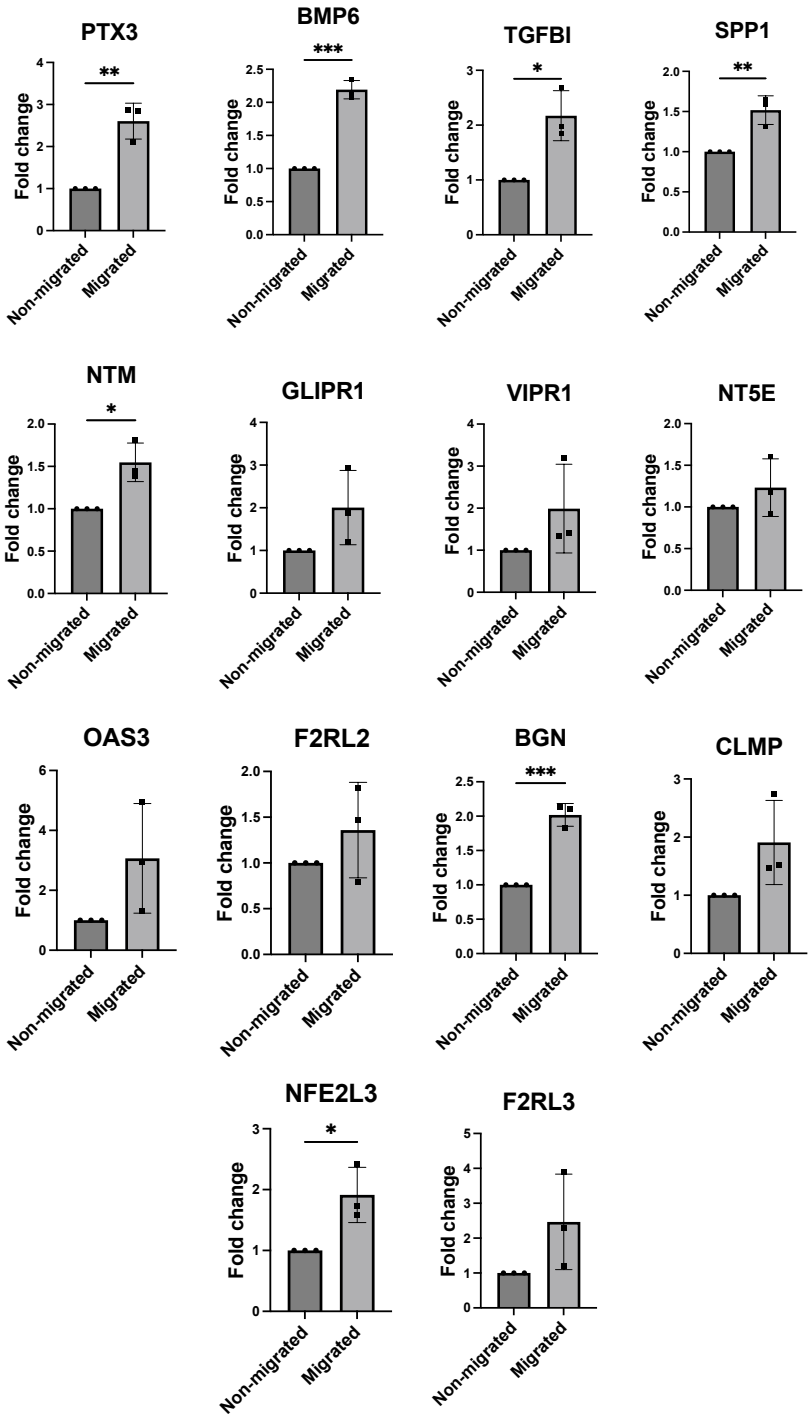

FIG S4: Differentially expressed gene verification comparing migrated hiPSC-CMs to their non-migrated counterparts. HiPSC-CM-A,-B and -C were seeded at day 15 on transwell inserts and exposed to MI 1:10 for 24h after which the non-migrated and migrated cells were harvested separately. RT-qPCR confirmed the upregulation of all 14 genes of interest in migrated cells compared to their non-migrated counterparts in all three biological replicates. Statistical analyses were performed using two-tailed, unpaired t-tests. Error bars indicate mean ± SD. *: $P \leq 0.05$, **: $P \leq 0.01$, ***: $P \leq 0.001$.

Figure S5

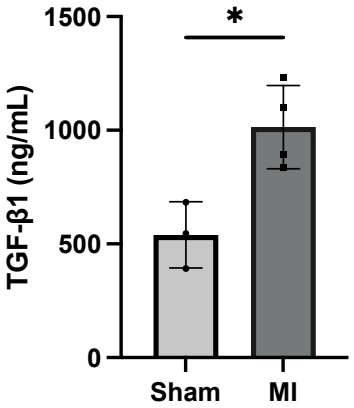

FIG S5: TGF-β1 levels in sham and MI rat left ventricular homogenates. TGF-β1 was measured in sham (n=3) or MI (n=4) LV homogenate samples by ELISA. Statistical analysis was performed using a two-tailed unpaired t-test. *, $P < 0.05$.

Table S1: Gene expression profiles of hiPSC-CMs analysed for bulk RNAseq after 24h of incubation with MI homogenate (1:10). Values represent normalised read counts. Padj = adjusted p-value or false discovery rate (FDR).

Gene	hiPSC-CM-A			hiPSC-CM-B		
	Migrated	Non-migrated	padj	Migrated	Non-migrated	padj
TNNT2	8071	18864	0.07	11685	16025	1
NKX2-5	3044	4933	0.48	3892	4316	1
MYL7	18495	44382	0.06	26798	38134	1
NR2F2	1109	487	0.10	746	540	1
MYL2	60	142	0.14	91	123	1
IRX4	126	254	0.23	291	257	1
TBX18	1193	779	0.56	206	85	0.59
HCN4	1458	2882	0.21	1097	1643	1
TNNI3	231	687	0.01	280	515	1
TNNI1	2620	6508	0.05	3499	5198	1
MYH6	26392	88865	0.003	14032	32149	0.53
MYH7	4489	16524	0.001	2285	4259	1
DDR2	806	403	0.21	599	284	0.84
THY1	368	149	0.07	30	5	0.23
ACTA2	5692	7015	0.86	1783	2130	1
CD31	-	-		-	-	

Table S2: Gene Ontology (GO) analysis of migrated versus non-migrated hiPSC-CM-Bs and hiPSC-CM-Cs after 24h of incubation with MI homogenate.

GOID	Description	GeneRatio	pvalue	padj
hiPSC-CM-A				
GO:0030198	extracellular matrix organization	86/1624	2.29E-15	1.20E-12
GO:0006935	chemotaxis	100/1624	2.08E-09	2.54E-07
GO:0042330	taxis	100/1624	2.34E-09	2.79E-07
GO:2000147	positive regulation of cell motility	90/1624	2.95E-09	3.45E-07
GO:0040017	positive regulation of locomotion	94/1624	3.75E-09	4.19E-07
GO:0031032	actomyosin structure organization	48/1624	8.57E-09	9.18E-07
GO:0030335	positive regulation of cell migration	86/1624	1.88E-08	1.90E-06
GO:0030048	actin filament-based movement	37/1624	1.93E-08	1.91E-06
GO:0060326	cell chemotaxis	41/1624	5.87E-05	0.002
GO:0050920	regulation of chemotaxis	36/1624	7.37E-05	0.002
GO:0050921	positive regulation of chemotaxis	25/1624	0.0003	0.005
GO:0006929	substrate-dependent cell migration	9/1624	0.001	0.01
GO:0042246	tissue regeneration	13/1624	0.001	0.01
GO:0014812	muscle cell migration	17/1624	0.005	0.04
hiPSC-CM-B				
GO:0006935	chemotaxis	25/421	0.0048	0.12
GO:0042330	taxis	25/421	0.0049	0.12
GO:2000147	positive regulation of cell motility	21/421	0.012	0.20
GO:0050921	positive regulation of chemotaxis	8/421	0.013	0.20
GO:0030335	positive regulation of cell migration	20/421	0.017	0.23
GO:0040017	positive regulation of locomotion	21/421	0.024	0.28
GO:0060326	cell chemotaxis	11/421	0.028	0.31

Table S3: Differentially expressed genes (DEGs) shared between migrated (A-M,B-M) versus non-migrated hiPSC-CM-A (A-NONM) and hiPSC-CM-B (B-NONM) after 24h of incubation with MI homogenate diluted 1:10. Values represent as normalised read counts. Padj = adjusted p-value or false discovery rate (FDR).

DEG	A-M	A-NONM	log2FC	padj A	B-M	B-NONM	log2FC	padj B
PTX3	4959.38	312.57	3.99	3E-13	1931.98	157.41	3.62	2E-10
SOX17	955.81	83.22	3.52	1E-09	160.50	23.36	2.77	0.0004
BMP6	1081.94	132.95	3.02	2E-07	161.49	32.50	2.31	0.008
TGFBI	9837.96	1522.27	2.69	2E-06	1024.09	229.51	2.16	0.002
SPP1	3503.99	565.27	2.63	3E-06	95.51	10.16	3.22	0.0004
NTM	936.10	133.96	2.80	2E-06	279.65	61.95	2.17	0.006
GLIPR1	1134.16	175.57	2.69	3E-06	192.02	49.76	1.95	0.034
VIPR1	144.85	13.19	3.44	2E-06	67.94	10.16	2.73	0.011
RGPD6	46.31	318.66	-2.78	1E-05	50.22	193.97	-1.95	0.031
NT5E	126.13	27.40	2.20	0.002	240.27	46.72	2.36	0.002
CASP4	217.77	48.71	2.16	0.001	81.73	13.20	2.62	0.009
OAS3	34.49	5.08	2.73	0.012	38.40	0.00	8.27	0.0002
F2RL2	434.55	113.66	1.93	0.002	151.64	31.48	2.26	0.011
BGN	319.26	77.13	2.05	0.001	93.55	17.27	2.43	0.012
CLMP	773.52	259.80	1.57	0.014	509.09	134.05	1.92	0.016
EPAS1	1503.68	459.73	1.71	0.005	208.76	49.76	2.07	0.016
NFE2L3	205.94	37.55	2.45	0.0002	222.54	53.82	2.05	0.016
KCNJ2	76.86	8.12	3.22	9E-05	55.14	8.13	2.74	0.020
KIF18B	692.72	157.30	2.14	0.0003	331.84	88.35	1.91	0.024
MKI67	1768.74	360.27	2.30	6E-05	986.67	286.38	1.78	0.029
HMGA2	11854.04	3122.68	1.92	0.001	5456.22	1629.94	1.74	0.029
VEPH1	59.12	15.22	1.95	0.029	97.48	21.33	2.19	0.029
F2RL3	79.81	23.34	1.77	0.030	100.44	22.34	2.16	0.030
CDK1	1067.16	276.04	1.95	0.001	606.57	176.70	1.78	0.034
SLC7A11	10478.46	3401.76	1.62	0.008	11840.03	3683.36	1.68	0.039
DACT2	102.48	21.31	2.26	0.002	17.72	0.00	7.16	0.044
NEK2	332.07	87.28	1.93	0.003	156.57	40.62	1.94	0.045
DHRS2	19.71	2.03	3.20	0.035	45.29	194.98	-2.10	0.014

Table S4. List of unconjugated antibodies used in this study. All antibodies are reactive against human. ICC: immunohistochemistry, WB: western blot, FC: flow cytometry.

Target	Host species	Source	Application	Working concentration
Oct3/4	Goat	R&D, #AF1759	ICC	1:50
Nanog	Goat	R&D, #AF1997	ICC	1:50
Sox2	Rabbit	Abcam, #Ab97959	ICC	1:500
Nkx2.5	Goat	R&D, #AF2444	ICC	1:20
cTNT	Mouse	Thermofisher, #MA5-12960	ICC, WB, FC	1:50
Sarcomeric alpha-actinin	Mouse	Sigma (Merck), #A7811	ICC	1:250
MLC2v	Rabbit	Proteintech, #10906-1-AP	FC	1:400

Table S5. List of conjugated antibodies used in this study. ICC: immuno-histochemistry, WB: western blot, FC: flow cytometry.

Target	Conjugate	Source	Application	Working concentration
Anti-mouse	AF488	Thermofisher, #A21202	ICC	1:500
Anti-mouse	AF647	Thermofisher, #A21242	FC	1:500
Anti-goat	AF488	Thermofisher, #A11055	ICC	1:500
Anti-goat	AF594	Thermofisher, #A11058	ICC	1:500
Anti-rabbit	AF488	Thermofisher, #A21206	ICC	1:500
Anti-rabbit	AF555	Thermofisher, #A32732	FC	1:500
Anti-rabbit	AF594	Thermofisher, #A11037	ICC	1:500
Anti-human TRA-1-81 (IgM, κ)	AF488	Biolegend, #330710	FC	1:10
Anti-human isotype (IgM, κ)	AF488	Biolegend, #401617	FC	1:10
Anti-human SSEA4 (IgG3)	AF488	Thermofisher, #53-8843-42	FC	1:10
Anti-human isotype (IgG3)	AF488	Biolegend, #401324	FC	1:10
Anti-human cTnT (IgG1)	FITC	Miltenyi, #130-119-575	FC	1:50
Anti-human isotype control (IgG1)	FITC	Miltenyi, #130-118-354	FC	1:50

Table S6: Forward and reverse primer sequences for the genes of interest for RT-qPCR. All primers have a melting temperature of approximately 60°C.

Gene	Primer sequence	
	Forward (5'-3')	**Reverse (5'-3')**
POU5F1	CAAAGCAGAAACCCTCGTGC	CTCGGACCACATCCTTCTCG
SOX2	GGGGAAAGTAGTTTGCTGCC	CGCCGCCGATGATTGTTATT
NANOG	CTGCAGAGAAGAGTGTCGCA	ACCAGGTCTTCACCTGTTTGT
MESP1	ACGGTCCCCGCTCCTTC	CAGTCTGCCAAGGAACCACT
KIT	AGGAAACGCTCGACTACCTG	CATTCCAGGATAGGGGCTGC
NKX2-5	CAAGTGTGCGTCTGCCTTTC	CGCACAGCTCTTTCTTTTCGG
TNNT2	ATCCTCTGCCTCACCCAGTC	GCTCTCCCTCAGAACAGCAG
MYL2	CAATTAACTTTACTGTGTTCCTCACAA	GAACGTAATCAGCCTTCAGCAC
MYL7	CCGTCTTCCTCACGCTCTT	TGAACTCATCCTTGTTCACCAC
PTX3	CGTCTCTCCAGCAATGCATC	AAGAGCTTGTCCCATTCCGA
BMP6	CCGACAACAGAGTCGTAATCGC	CTGCCATCCCAGGTCTTGGAAA
TGFBI	ATGACCCTCACCTCTATGTACC	CACAGTTCACAGTTACAATCCCA
SPP1	GCCGAGGTGATAGTGTGGTT	AACGGGGATGGCCTTGTATG
NTM	TGCTGTTCCTTGTACCCACAGG	CGAGGATCCAGGCACCACT
GLIPR1	GGCTTTGACGCTCTTTCCAA	CGTTTGACTTGGTCTCGCTGT
VIPR1	GGACACCATCAACTCCTCACTG	CGCAGTTTCTGAAGCAGGATTCG
NT5E	TCTTCTAAACAGCAGCATTCC	CATTTCATCCGTGTGTCTCAG
OAS3	CCTGATTCTGCTGGTGAAGCAC	TCCCAGGCAAAGATGGTGAGGA
F2RL2	TCCTGGTGTTTGTAGTTGGTGT	CCAGTTGTTCCCATTGAGATGA
BGN	TGACTGGCATCCCCAAAGAC	GAGTAGCGAAGCAGGTCCTC
CLMP	TTACTGGCAGCGAATCCGAGAG	CTGGTACAGTCCAGAGTAGGAC
NFE2L3	CCAGTTGCTTTCATCACAGCCTG	CACATCCTGACTTATAGCCTGGC
F2RL3	ACCGGAGGTGGTGATGACAG	CACAGACTTGGCCTGGGTAG
GAPDH	GTCAAGGCTGAGAACGGGAA	AAATGAGCCCCAGCCTTCTC
ACTB	GTGGCATCCACGAAACTACC	GTACTTGCGCTCAGGAGGAG